Analyzing the Onset of Cometary Activity by the Jupiter-family Comet 2023 RN₃

Matthew M. Dobson[1] , Megan E. Schwamb[1] , Alan Fitzsimmons[1] , Michael S. P. Kelley[2] , Carrie E. Holt[3] ,
Joseph Murtagh[1] , Henry H. Hsieh[4,5] , Larry Denneau[6] , Nicolas Erasmus[7,8] , A. N. Heinze[9] , Luke J. Shingles[1,10] ,
Robert J. Siverd[6] , Ken W. Smith[1] , John L. Tonry[6] , Henry Weiland[6] , David. R. Young[1] , Tim Lister[3] ,
Edward Gomez[11] , Joey Chatelain[3] , and Sarah Greenstreet[9,12]

[1] Astrophysics Research Centre, School of Mathematics and Physics, Queen's University Belfast, Belfast BT7 1NN, UK; mdobson04@qub.ac.uk
[2] Department of Astronomy, University of Maryland, College Park, MD 20742-0001, USA
[3] Las Cumbres Observatory, 6740 Cortona Drive, Suite 102, Goleta, CA 93117, USA
[4] Planetary Science Institute, 1700 East Fort Lowell Road, Suite 106, Tucson, AZ 85719, USA
[5] Institute of Astronomy and Astrophysics, Academia Sinica, P.O. Box 23-141, Taipei 10617, Taiwan
[6] Institute for Astronomy, University of Hawaii at Manoa, Honolulu, HI 96822, USA
[7] Department of Physics, Stellenbosch University, Stellenbosch 7602, South Africa
[8] South African Astronomical Observatory, Cape Town 7925, South Africa
[9] Department of Astronomy and the DIRAC Institute, University of Washington, 3910 15th Avenue NE, Seattle, WA 98195, USA
[10] GSI Helmholtzzentrum für Schwerionenforschung, Planckstraße 1, 64291 Darmstadt, Germany
[11] Las Cumbres Observatory, School of Physics and Astronomy, Cardiff University, Queens Buildings, The Parade, Cardiff CF24 3AA, UK
[12] Rubin Observatory/NSF NOIRLab, 950 N. Cherry Avenue, Tucson, AZ 85719, USA

Abstract

We utilize serendipitous observations from the Asteroid Terrestrial-impact Last Alert System (ATLAS) and the Zwicky Transient Facility in addition to targeted follow-up observations from the Las Cumbres Observatory (LCO) and Liverpool Telescope to analyze the first observed instance of cometary activity by the newly discovered Jupiter-family comet C/2023 RN₃ (ATLAS), whose orbital dynamics place it close to residing on a Centaur-like orbit. Across our 7 month baseline, we observe an epoch of cometary activity commencing in 2023 August with an increase in brightness of >5.4 mag. The lightcurve of 2023 RN₃ indicates the presence of continuous cometary activity across our observations, suggesting the onset of a new period of sustained activity. We find no evidence of any outbursts on top of the observed brightening nor do we find any significant color evolution across our observations. 2023 RN₃ is visibly extended in LCO and Liverpool Telescope observations, indicating the presence of a spatially extended coma. Numerical integration of 2023 RN₃'s orbit reveals the comet to have recently undergone a slight increase in semimajor axis due to a planetary encounter with Jupiter; however, whether this orbital change could trigger 2023 RN₃'s cometary activity is unclear. Our estimate for the maximum dust production metric of $Af\rho \sim 400$ cm is consistent with previous measurements for the Jupiter-family comet and Centaur populations.

Unified Astronomy Thesaurus concepts: Comets (280); Comae (271); Small Solar System bodies (1469); Centaur group (215); Broad band photometry (184); Wide-field telescopes (1800); Orbital evolution (1178)

Materials only available in the online version of record: figure sets, machine-readable table

1. Introduction

C/2023 RN₃ (ATLAS; hereafter referred to as "2023 RN₃") is a Jupiter-family comet (JFC) recently discovered by the Asteroid Terrestrial-impact Last Alert System (ATLAS; J. L. Tonry et al. 2018a, 2018b) wide-field sky survey on 2023 September 4 (D. W. E. Green 2023) during an epoch of cometary activity that caused it to brighten by more than 4 mag (H. H. Hsieh et al. 2023). Early analysis of 2023 RN₃'s cometary activity by H. H. Hsieh et al. (2023) revealed the presence of a visible coma. With a semimajor axis $a = 10.147$ au, perihelion $q = 5.172$ au (last passed on 2023 January 16), eccentricity $e = 0.490$, and inclination $i = 10.358$ deg, 2023 RN₃'s orbit is that of a JFC, with a Tisserand parameter $T_J = 2.907$. However, its perihelion and Tisserand parameter values lie close to the threshold values ($q = 5.2$ au, D. Jewitt 2009; B. Gladman et al. 2008; and $T_J = 3.05$, B. Gladman et al. 2008, respectively) that separate the JFC population from the Centaurs, small icy objects on chaotic orbits in the giant planet region of the solar system that are thought to replenish the JFC population, making the study of 2023 RN₃ relevant to studies of both JFCs and Centaurs.

Both Centaurs and JFCs are known to exhibit cometary activity (D. Jewitt 2009; M. S. Kelley & D. H. Wooden 2009; J. M. Bauer et al. 2013; N. Peixinho et al. 2020; D. Jewitt & H. H. Hsieh 2022), manifesting as dust comae and tails. This activity can take the form of "outbursts," sudden and brief increases in the mass loss and corresponding brightness of the object (D. W. Hughes 1990). However, while the activity of JFCs is closely coupled with their proximity to perihelion, the activity exhibited by Centaurs can occur throughout their orbits (N. Peixinho et al. 2020). This points to different mechanisms responsible for activity exhibited by both populations. The activity of JFCs is generally due to the sublimation of water ice for those with perihelia interior to ~ 3 au (K. J. Meech & J. Svoren 2004; M. Womack et al. 2017), with sublimation of CO and CO_2 thought to be the dominant driver of JFC activity exterior to this distance (T. Ootsubo et al. 2012; A. L. Cochran et al. 2015). By comparison, the mechanism responsible for Centaur activity is not as well understood. Proposed causes of Centaur activity include newly exposed pockets of volatile

Table 1
Number and Time Ranges of Observations of 2023 RN$_3$ for Each Filter Used in Our Analysis

Telescope/Survey	Filter	Start Date (YYYY-MM-DD)	End Date (YYYY-MM-DD)	Number of Observations
ATLAS	c	2023-07-18	2023-12-10	36
ATLAS	o	2023-06-06	2023-12-16	106
ZTF	ZTF-g	2023-08-03	2023-11-13	26
ZTF	ZTF-r	2023-08-03	2024-01-05	28
Liverpool Telescope	SDSS-g'	2023-12-08	2023-12-14	6
Liverpool Telescope	SDSS-r'	2023-11-26	2023-12-14	11
Liverpool Telescope	SDSS-i'	2023-11-26	2023-12-14	12
LOOK	PS1 w	2023-11-17	2023-11-17	4
LOOK	SDSS-g'	2023-11-16	2024-01-10	26
LOOK	SDSS-r'	2023-11-16	2024-01-10	24
LOOK	SDSS-i'	2023-11-26	2024-01-10	19
Total		2023-06-06	2024-01-10	298

surface ices (D. Prialnik 1992) or volatiles released by the amorphous-to-crystalline transition of subsurface water ice (D. Jewitt 2009). Furthermore, analysis of Centaur orbital dynamics points to correlations between the activity exhibited by a Centaur and its perihelion (D. Jewitt 2009; E. Lilly et al. 2021), its lifetime in the giant planet region (J. A. Fernández et al. 2018), and its evolutionary history, with active Centaurs tending to have encountered a giant planet in the last ~10^3 yr of its history, causing an abrupt decrease in its semimajor axis (J. A. Fernández et al. 2018; E. Lilly et al. 2021, 2024). Understanding the mechanism behind Centaur activity, and how this activity transitions to that exhibited by JFCs, is thus an important step in understanding cometary evolution in the solar system.

In this paper, we analyze the 2023 cometary activity of 2023 RN$_3$, combining follow-up observations from Las Cumbres Observatory (LCO; T. M. Brown et al. 2013) as part of the Las Cumbres Observatory Outbursting Objects Key (LOOK; T. Lister et al. 2022) project and the Liverpool Telescope (I. A. Steele et al. 2004) along with serendipitous observations from ATLAS and the Zwicky Transient Facility (ZTF; E. C. Bellm et al. 2019; M. J. Graham et al. 2019). This paper is structured as follows: In Section 2, we briefly describe the observations used in our analysis and photometry. In Section 3, we present our analysis and findings studying the evolution in the brightness, color, radial profile, and dust production of 2023 RN$_3$. We present our summary and conclusions in Section 4.

2. Observations and Data Reduction

Our data set consists of both targeted follow-up observations of 2023 RN$_3$ (LOOK and Liverpool Telescope) and serendipitous observations of the object from automated surveys (ATLAS and ZTF). Our observations, summarized in Table 1, extend in time from 2023 June 6 to 2024 February 2. The serendipitous observations from ATLAS and ZTF make up the majority of our data set and cover the onset of 2023 RN$_3$'s cometary activity first observed on 2023 August 26 (see Section 3.1). Our observations from LOOK and Liverpool Telescope sample 2023 RN$_3$ after its activity commenced.

2.1. ATLAS

ATLAS regularly observes the entire night sky to a limiting magnitude of 19.5 mag using 30 s exposures in two non-standard filters, cyan (c, 420–650 nm) and orange

(o, 560–820 nm; J. L. Tonry et al. 2018a). ATLAS consists of four telescope units, two of which are located in Hawai'i (Mauna Load and Haleakala), one in Chile (El Sauce), and one in South Africa (Sutherland). Each of the four ATLAS units consists of a 0.5 m Schmidt telescope with a field of view (FOV) of 28.9 deg^2 with a pixel scale of $1''86$ pixel^{-1} (J. L. Tonry et al. 2018a, 2018b). Further details of ATLAS and its data reduction pipeline can be found in J. L. Tonry et al. (2018a, 2018b) and K. W. Smith et al. (2020). We use both c and o filter observations of 2023 RN$_3$ from all four ATLAS telescopes between 2023 June 6 and 2024 February 2. We utilize the difference images automatically generated by the ATLAS reduction pipeline for each observation to reduce the effect of contamination from background flux sources (e.g., stars, galaxies) on our photometry of 2023 RN$_3$.

2.2. ZTF

Using the 48 inch (1.2 m) Samuel Oshin telescope, ZTF is a wide-field time domain survey that has been observing the visible sky since 2017 October with a cadence of approximately 3 days. Each observation has an exposure time of 30 s, with an FOV of 43 deg^2 and a pixel scale of $1''01$ pixel^{-1}, and is obtained using three broadband filters ZTF-g, ZTF-r, and ZTF-i. Further details of ZTF, its system overview, survey strategy, data processing pipeline, and science objectives can be found in E. C. Bellm et al. (2019), M. J. Graham et al. (2019), and F. J. Masci et al. (2019). We query the ZTF observations of 2023 RN$_3$ via the Infrared Science Archive (IRSA) of the NASA Infrared Processing and Analysis Center (IPAC), which utilizes the Jet Propulsion Laboratory (JPL) Horizons[13] ephemeris of a queried object to obtain all ZTF observations that coincide with the position of that object. These observations range in time from 2023 August 3 to 2024 January 7 in the broadband filters ZTF-g and ZTF-r.

2.3. LOOK

The LCO 1.0 m telescopes (T. M. Brown et al. 2013) observed 2023 RN$_3$ from 2023 November 26 to 2024 January 10 (including the observations reported in H. H. Hsieh et al. 2023) as part of LOOK (T. Lister et al. 2022). Observations were taken in Sloan Digital Sky Survey (SDSS) g, r, and i filters (K. C. Chambers et al. 2016) with the original

---

[13] https://ssd.jpl.nasa.gov

H. H. Hsieh et al. (2023) observations in the *w*-filter included in our analysis. Observations were scheduled with the NEOExchange web portal (T. A. Lister et al. 2021). Each 1 m telescope utilizes an identical Sinistro imager comprising a Fairchild 4096 × 4096 pixel charge-coupled device (CCD) with an FOV of 26′.6 × 26′.6, resulting in a pixel scale of 0″.387 pixel^{-1} (T. M. Brown et al. 2013). To ensure negligible on-sky motion of 2023 RN$_3$ within this pixel scale, all observations were obtained with the telescope in half-rate tracking mode, with exposure times of 245 s. These observations are automatically processed using the LCO image processing pipeline "Beautiful Algorithm to Normalize Zillions of Astronomical Images" (BANZAI; C. McCully et al. 2018). The LOOK photometry pipeline includes automatic calibration of observations to the Pan-STARRS1 photometric system (J. L. Tonry et al. 2012) using the ATLAS-RefCat2 all-sky photometric catalog (J. L. Tonry et al. 2018b), the CALVIACAT software (M. Kelley & T. Lister 2021), and background field stars measured with BANZAI (T. Lister et al. 2022). Due to the difference between the Pan-STARRS1 filter system of ATLAS-RefCat2 and the SDSS filter system of LCO, the LOOK photometry pipeline performs a color correction to transform the instrumental magnitudes to their corresponding Pan-STARRS1 filters g', r', and i' (T. Lister et al. 2022). Of these observations, we utilize for our analysis only those that were obtained with seeing ⩽4″.

2.4. Liverpool Telescope

The Liverpool Telescope is a 2 m robotic telescope located at the Observatorio del Roque de los Muchachos, La Palma, Canary Islands (I. A. Steele et al. 2004). We obtained observations of 2023 RN$_3$ between 2023 November 26 and 2023 December 14 using the IO:O wide-field camera (R. M. Barnsley et al. 2016) whose 4096 × 4112 pixel CCD results in an FOV of 10′ × 10′. Observations were obtained in SDSS *r* and *i* filters for conditions of airmass <2.0 and seeing <2″.0. We utilize sidereal tracking of 2023 RN$_3$, with exposure times of 82 s for *g*-filter observations and 70 s in *r* and *i* filters to ensure negligible on-sky motion of the object within the 0″.3 pixel^{-1} resolution afforded by 2 x 2 pixel binning. Observations were automatically reduced via the IO:O reduction pipeline. We analyze 2023 RN$_3$ in the 29 observations where it was detected above 3σ.

3. Analysis and Results

Our multiwavelength observations from ATLAS, ZTF, LOOK, and Liverpool Telescope allow us to analyze 2023 RN$_3$'s 2023 cometary activity. We use the multimonth, multiwavelength baseline observations from ATLAS, ZTF, and LOOK to explore the evolution of 2023 RN$_3$'s measured brightness and determine any evolution of its observed color. We use the high-resolution LOOK and Liverpool Telescope observations to analyze 2023 RN$_3$'s surface brightness distribution across time. Finally, we utilize our ATLAS, ZTF, and LOOK observations to estimate 2023 RN$_3$'s activity level across our observational baseline.

3.1. Brightness Evolution

Using our largest data sets, ATLAS, ZTF, and LOOK, we examine the brightness evolution of 2023 RN$_3$. To account for the visible extension exhibited by 2023 RN$_3$ as reported by

H. H. Hsieh et al. (2023), we perform aperture photometry on all our observations with a sufficiently large aperture, applying an effective radius of 20,000 km, corresponding to an angular size of 4″.83 to 6″.36 across our observations. We use the aperture photometry automatically calculated by the LOOK photometry pipeline (T. Lister et al. 2022). For our ATLAS and ZTF observations, we use Source Extractor Python (E. Bertin & S. Arnouts 1996; K. Barbary 2016) to identify sources. We identify the closest source as 2023 RN$_3$ within a threshold distance (3″ for ATLAS observations, 1″.5 for ZTF, due to the differing pixel scales of both surveys) from 2023 RN$_3$'s predicted position by JPL Horizons. We use the *photutils* Python library (L. Bradley 2023) to perform aperture photometry on 2023 RN$_3$, applying a circular aperture. The background annulus apertures had inner and outer radii of 4 and 5 times the circular aperture radius, 20,000 km, respectively. We apply per observation the zero-points reported from the ATLAS (J. L. Tonry et al. 2018b) and ZTF (F. J. Masci et al. 2019) photometry pipelines. If the flux measured for 2023 RN$_3$ has a signal-to-noise ratio (SNR) of <3, or if no source is found by Source Extractor Python, we calculate a 3σ upper limit $m_{3\sigma}$ from forced photometry at the predicted coordinates of 2023 RN$_3$ according to the following equation:

$$M_{3\sigma} = -2.5 \log_{10}(3 * dF) + ZP, \tag{1}$$

where dF is the uncertainty in the measured flux and ZP is the observation zero-point magnitude. Table 2 lists the magnitude measurements (or 3σ upper limits) of 2023 RN$_3$ for each observation on which we performed photometry.

To transform our magnitude measurements to the same wavelength, we select the ATLAS *o* filter data set as our standard filter on account of it having the largest number of observations and the longest time baseline, calculating and applying a color offset to the other data sets (listed in Table 3). Magnitude offsets were calculated from the difference in median apparent magnitude between a given filter and the ATLAS *o* filter across their overlapping time span. For each color-corrected magnitude value, we query JPL Horizons for the corresponding geocentric and heliocentric distances of 2023 RN$_3$ at the time of observation and transform the apparent magnitudes of 2023 RN$_3$ into reduced magnitudes (the apparent magnitude scaled to geocentric and heliocentric distances of 1 au). Figure 1 shows the apparent magnitude lightcurves of 2023 RN$_3$ in each filter, with the magnitudes standardized for the *o* filter shown in Figure 2. The serendipitous data sets from ATLAS and ZTF allowed them to sample the rise of 2023 RN$_3$'s brightness, with ZTF making the first detection on 2023 August 26 and ATLAS making the last nondetection on 2023 August 21; targeted follow-up observations from LOOK were scheduled after the object was detected. Figures 1 and 2 show that over the course of 137 days, 2023 RN$_3$ suddenly increased in brightness at an initial rate of approximately 0.36 mag day^{-1}, reaching a peak apparent brightness of ∼17.5 mag, and has since leveled off to a constant magnitude after a slight decrease in brightness. This indicates that cometary activity may be continuing across this period and that 2023 RN3's increase in brightness is the onset of an epoch of continuous cometary activity. Extrapolating 2023 RN$_3$'s initial brightening rate to the 3σ limiting magnitude from H. H. Hsieh et al. (2023) of 22.5 mag, which we assume to be the nuclear apparent magnitude of 2023 RN$_3$,

Table 2
Apparent Magnitudes of 2023 RN$_3$ in Each Observation from ATLAS, ZTF, and LOOK

MJD	Magnitude (mag)	Magnitude Uncertainty (mag)	Photometry Flag	Filter	Heliocentric Distance (au)	Geocentric Distance (au)	Phase Angle (deg)	Survey
60191.567824	17.683	0.084	1	o	5.312	4.377	4.5017	ATLAS
60191.571448	17.875	0.100	1	o	5.312	4.377	4.5011	ATLAS
60191.604028	17.783	0.099	1	o	5.312	4.377	4.4952	ATLAS
60204.173872	17.677	0.065	1	o	5.327	4.339	2.1776	ATLAS
60204.177039	17.635	0.062	1	o	5.327	4.339	2.1770	ATLAS
60204.179792	17.821	0.087	1	o	5.327	4.339	2.1765	ATLAS
60204.210026	17.660	0.071	1	o	5.327	4.339	2.1711	ATLAS
60213.104433	17.628	0.108	1	o	5.339	4.339	0.9948	ATLAS
60213.127136	17.588	0.101	1	o	5.339	4.339	0.9942	ATLAS
60213.140634	17.678	0.108	1	o	5.339	4.339	0.9939	ATLAS

Note. Flag indicates if brightness measurement is the measured magnitude (flag = 1) or a 3σ upper limit (flag = 0).

(This table is available in its entirety in machine-readable form in the online article.)

Table 3
Magnitude Offsets for 2023 RN$_3$ Apparent Magnitudes in Each Filter,
Correcting to the ATLAS o Filter

Filter	Magnitude Offset (mag)
ATLAS c	−0.563
ATLAS o	0.000
PS1 g (ZTF)	−0.546
PS1 r (ZTF)	0.063
PS1 w (LOOK)	0.164
PS1 g' (LOOK)	−0.593
PS1 r' (LOOK)	−0.016
PS1 i' (LOOK)	0.097

we estimate the activity likely started within about 10 days of the first ZTF detection on 2023 August 26. Our observed brightness maximum, combined with the limiting magnitude measurement from H. H. Hsieh et al. (2023), would imply a total increase in brightness of $\Delta m > 5.4$ mag, comparable to that observed for the large cometary outbursts of the Centaur 29P/Schwassman-Wachmann 1 (J. M. Trigo-Rodríguez et al. 2008; R. Miles 2016; Z.-Y. Lin 2023) and the comet 12P/Pons-Brooks (F. Manzini et al. 2023; J. M. Trigo-Rodríguez et al. 2024). From visual inspection of our reduced magnitude lightcurve, we do not see evidence of any secondary cometary outbursts by 2023 RN$_3$ with its brightness evolution consistent with a single sudden rise in brightness followed by a small decrease to a relatively constant magnitude. Our 3σ upper limits before 2023 August 26 preclude an epoch of cometary activity as bright as the observed 2023 epoch; however, we cannot rule out lower-level cometary activity occurring before this date.

3.2. Color Evolution

We use the dual filter coverage of ATLAS, ZTF, and LOOK to search for any changes in 2023 RN$_3$'s $c - o$ or $g - r$ color across time. As per Section 3.1, for each magnitude measurement we use the geocentric and heliocentric distances of 2023 RN$_3$ at the time of observation to calculate the corresponding reduced magnitude. We apply the two methods used in

M. M. Dobson et al. (2024) for measuring color evolution for a varying lightcurve.

The first method involves binning all the magnitude measurements from a given data set by epoch of observation. ATLAS measurements that are separated in time by <2 days (its approximate observation cadence) are counted as part of an epoch. For ZTF and LOOK, there are often both g and r observations on the same night; thus, we consider magnitude measurements separated by <0.5 days as part of one epoch. For each epoch, if observations in both filters are present, the mean reduced magnitude of each filter is calculated, and with its associated uncertainty calculated as the standard deviation of the magnitudes in each filter. The corresponding $c - o$ or $g - r$ color index of each is calculated by subtracting these mean magnitudes, with the associated uncertainties propagated in quadrature.

The second method involves fitting polynomial splines to the magnitude values of a given filter for a given survey, allowing us to account for any sudden change in 2023 RN$_3$'s brightness across time. To ensure well-constrained polynomial fits, we only fit ZTF g and r observations before MJD 60270 due to the scarcity of data in these filters after these dates. Our ATLAS c filter has too few measurements to sufficiently constrain the value this way; therefore, we do not include it in our analysis. For each filter, we generate 10^3 data sets of synthetic magnitudes. We create a synthetic magnitude data set by duplicating the measured magnitude values and adding to each magnitude value a random number generated from a Gaussian distribution centered on zero with a standard deviation equal to the measured magnitude's uncertainty. We then fit a third-order polynomial spline to each set of synthetic magnitude values. For a given magnitude measurement in a given filter, we calculate 2023 RN$_3$'s magnitude in the other filter at the same time of measurement as predicted by its fitted spline. These two magnitude measurements are then used to calculate 2023 RN$_3$'s $(g - r)$ color at that time. This method is repeated for each of the 10^3 synthetic data sets.

Figure 3 shows the resulting ZTF and LOOK color indices across time, calculated from binning data by epoch of observation. The ZTF and LOOK color indices calculated from the spline fitting method are shown in Figures 4 and 5, respectively. We see no significant change in color across our
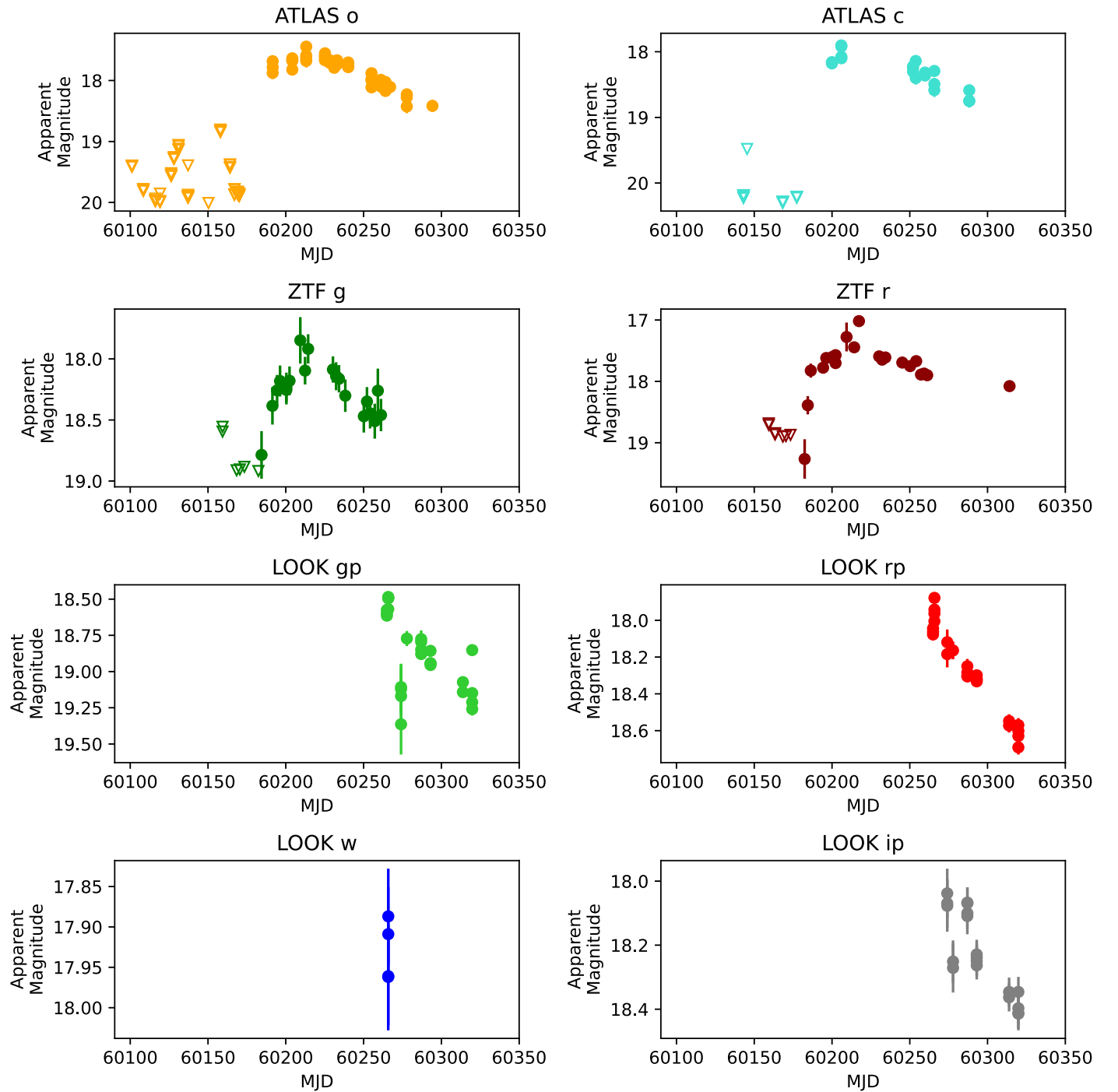
Figure 1. Lightcurve of 2023 RN$_3$ (apparent magnitude across time) in each filter. Filled circles indicate magnitude measurements; open triangles indicate 3σ upper limits.

baseline of observation, with its $c - o$ and $g - r$ color indices remaining constant within uncertainties. The mean $c - o$ from ATLAS, calculated from spline fitting, is 0.316 ± 0.023 with a median of 0.317. From binning our observations by epoch of observation, the mean $g - r$ values from ZTF and LOOK are 0.559 ± 0.044 and 0.597 ± 0.029 in their respective filter systems, with medians of 0.553 and 0.556, respectively. When fitting our observations with splines, the mean $g - r$ values from ZTF and LOOK in their respective filter systems are 0.601 ± 0.023 and 0.592 ± 0.008, with medians of 0.583 and 0.559, respectively. Our $g - r$ values for each filter system are

consistent to $<2\sigma$ for both methods and are also consistent with the color measured by H. H. Hsieh et al. (2023), $g - r = 0.61 \pm 0.03$. For comparison, the corresponding solar color indices in these filter systems are $(c - o) = 0.29$ and $(g - r)_{PS1} = 0.39$ (J. L. Tonry et al. 2018a; C. N. A. Willmer 2018). Hence, assuming our data to be dominated by a coma as evidenced by both the comet's fuzzy appearance in previous observations (H. H. Hsieh et al. 2023) and the large increase in the comet's brightness, the color of 2023 RN$_3$'s coma is significantly redder than the Sun and similar to previously observed cometary dust comae (M. Solontoi et al. 2012).
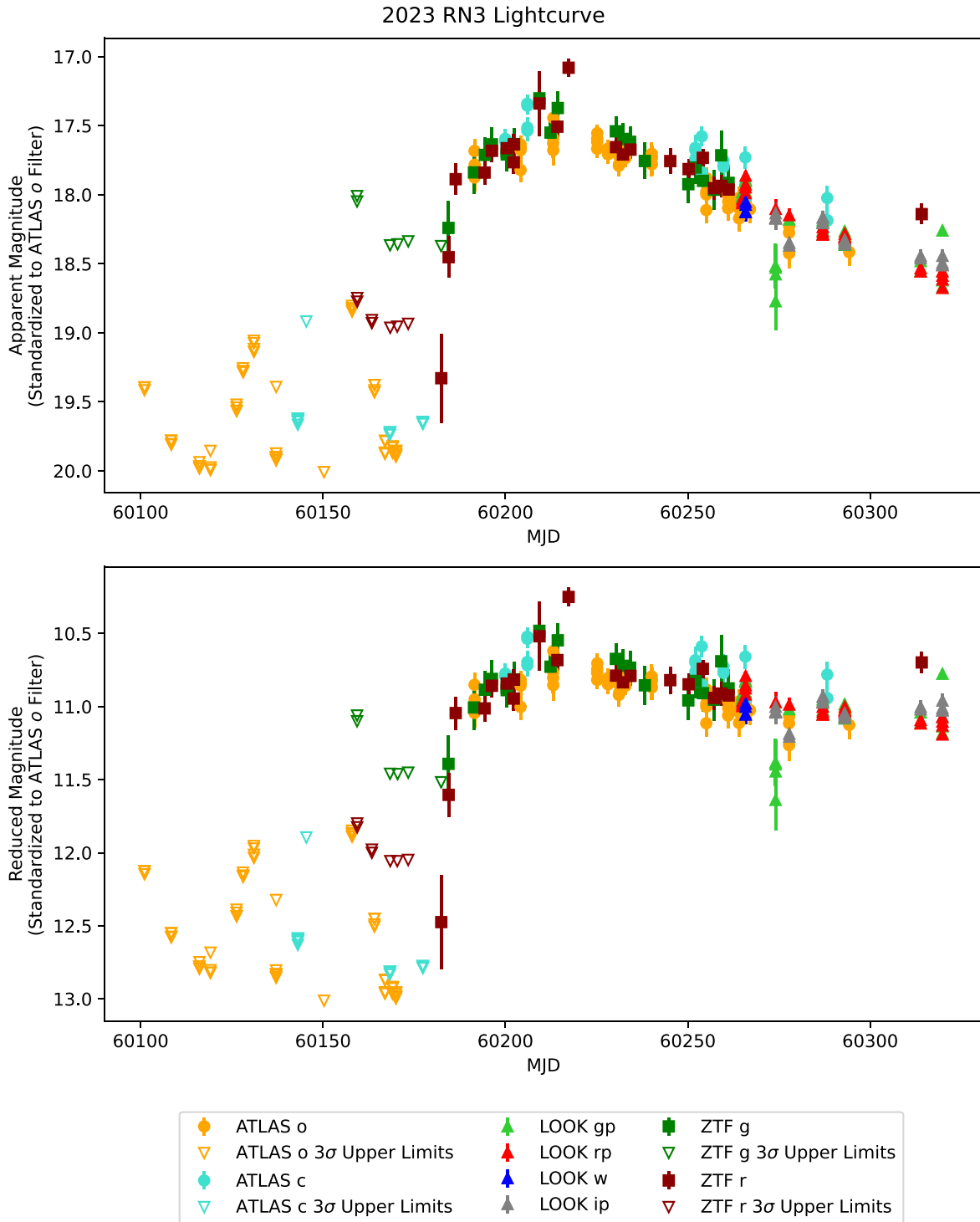
Figure 2. Lightcurve of 2023 RN₃ plotting apparent magnitude (top) and reduced magnitude (bottom) across time. All magnitudes are corrected to the ATLAS o filter wavelength. Filled markers indicate magnitude measurements of SNR $\geqslant 3$; open markers indicate 3σ upper limits.

3.3. Surface Brightness Evolution

The increased spatial resolution of the 2023 RN₃ observations from LOOK and Liverpool Telescope (0.39 and $0\rlap{.}{''}30\,\mathrm{pixel}^{-1}$, respectively) compared to ATLAS and ZTF (1.86 and $1\rlap{.}{''}01\,\mathrm{pixel}^{-1}$, respectively) allow us to analyze the structure of 2023 RN₃'s point-spread function (PSF) and investigate its evolution across time. We use our photometric detections of 2023 RN₃ where the comet's SNR is $\geqslant 26$ to enable accurate analysis of its radial profile. We utilize Source

Extractor Python (E. Bertin & S. Arnouts 1996; K. Barbary 2016) to detect background field stars from the Pan-STARRS Mean DR2 catalog (K. C. Chambers et al. 2016; H. A. Flewelling et al. 2020; E. A. Magnier et al. 2020) and select the stars that satisfy the following criteria: (1) they are isolated sources i.e., no other detected source lies within $10''$ of their centroid to prevent contamination; (2) the difference between their Pan-STARRS Mean DR2 PSF magnitudes and Kron magnitudes in the i filter is less than 0.05 mag to separate stars from
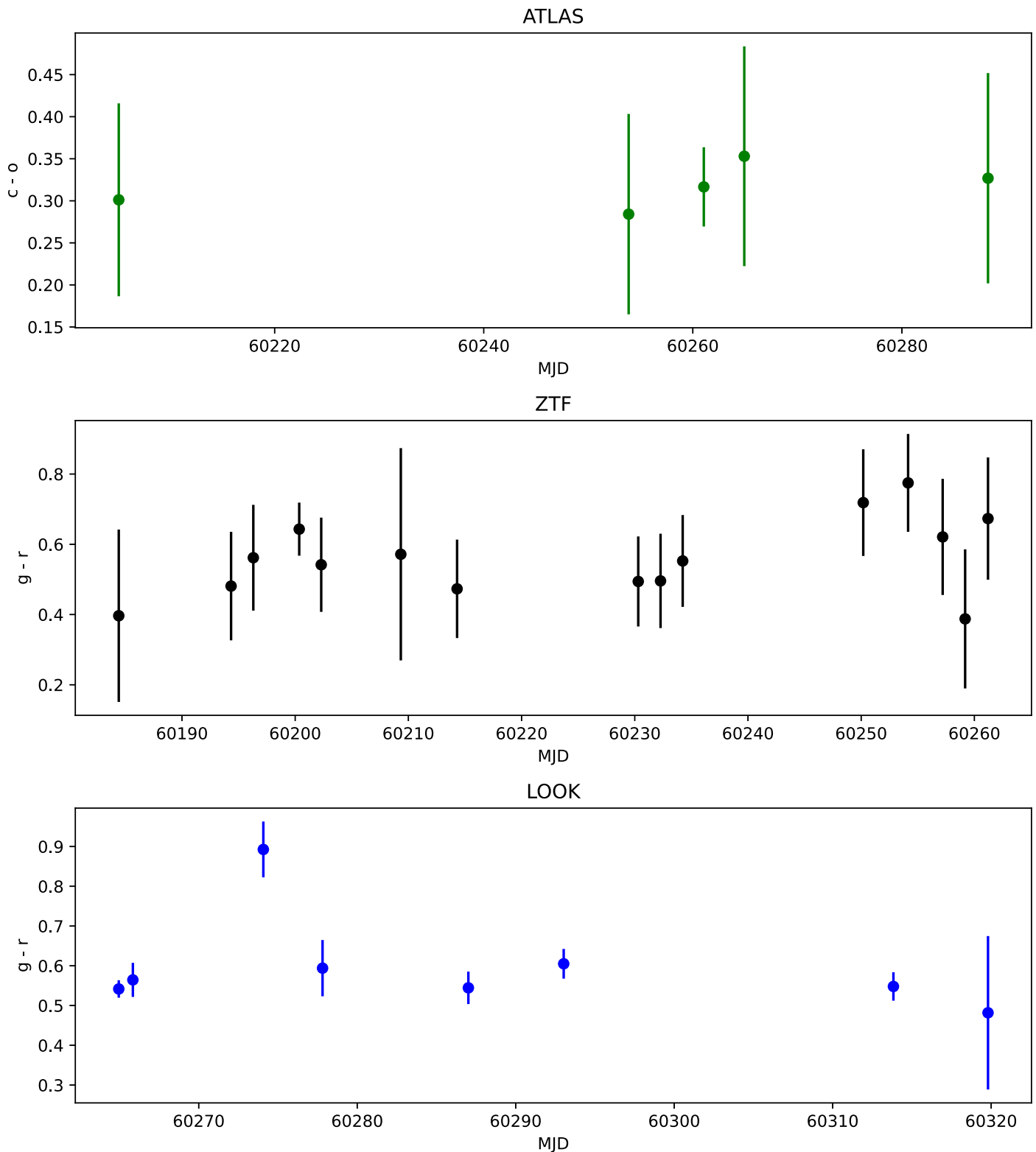
Figure 3. ATLAS $c - o$ (upper), ZTF $g - r$ (center), and LOOK $g - r$ (lower) color index values calculated from binning observations by epoch plotted across time.

galaxies; and (3) their g-filter Pan-STARRS Mean DR2 PSF magnitude is brighter than 20th mag to ensure they are of comparable brightness to 2023 RN$_3$. We then select the 10 stars whose peak fluxes as measured with Source Extractor Python are closest to that of 2023 RN$_3$ to compare to the comet. We use the *RadialProfile* function of the *photutils* Python library (L. Bradley 2023) to measure the radial profile of 2023 RN$_3$ in

comparison to the background stars, utilizing the background flux value calculated using the *Background* function from Source Extractor Python to remove the background noise contribution from each radial profile.

Figures 6 and 7 show, respectively, LOOK and Liverpool Telescope observations of 2023 RN$_3$ and for comparison a field star with a similar peak flux, their corresponding contour plots,
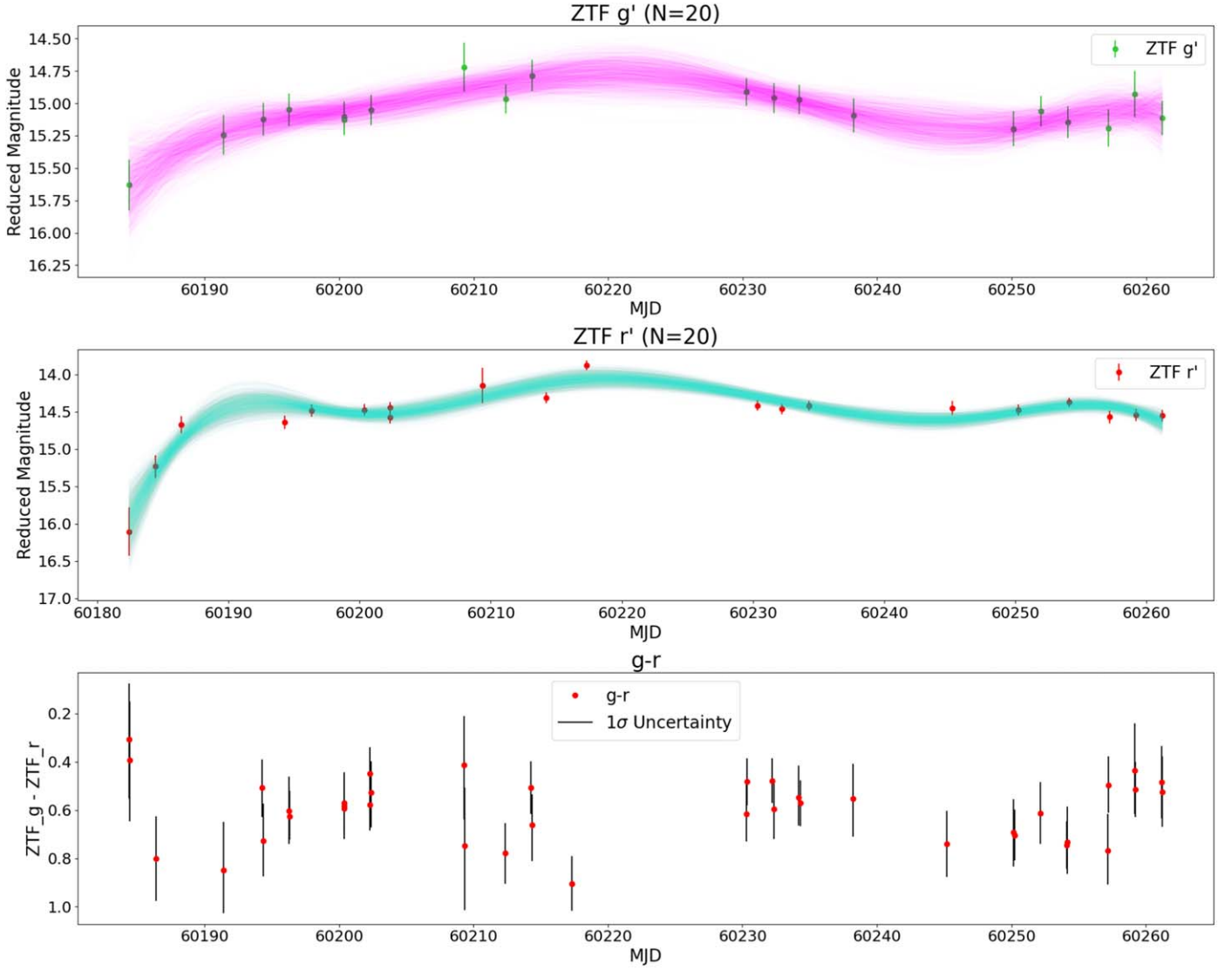
Figure 4. Top: ZTF *g*-filter reduced magnitudes (green circles) vs. time with third-order interpolated splines fitted to synthetic data overplotted (green). Middle: ZTF *r* filter reduced magnitudes (red circles) vs. time with third-order interpolated splines fitted to synthetic data overplotted (turquoise). Bottom: *g* − *r* color index value calculated from the predicted magnitudes in each filter from the synthetic magnitudes plotted across time. Red circles denote nominal color index values with green lines highlighting the range that includes the central 68.3% of synthetic values.

and the radial profile of 2023 RN$_3$ as compared to the 10 field stars of similar brightness, with the linear fit to the profile of 2023 RN$_3$ overplotted. The complete set(s) of contour plots are available online as figure sets. We calculate the full width half maximum (FWHM) of 2023 RN$_3$ and the comparison stars using the following equation:

$$\text{FWHM} = 2\sqrt{\ln(2)(a^2 + b^2)}, \qquad (2)$$

where *a* and *b* are the semimajor and semiminor axes of the fitted PSF to a given source detected by Source Extractor Python. The FWHM of 2023 RN$_3$ and the mean FWHM of the 10 comparison stars for each LOOK and Liverpool Telescope observation are included in the caption of each corresponding figure in the figure sets of Figures 6 and 7. We find that for each observation, the FWHM of 2023 RN$_3$ is extended compared to that of the background field stars and/or the radial profile of 2023 RN$_3$ deviates from the background star profile. This

indicates the presence of a spatially extended coma, consistent with the findings of H. H. Hsieh et al. (2023).

3.4. Afρ

To examine 2023 RN$_3$'s dust-production rate, we use the parameter *Af*ρ, introduced by M. F. A'Hearn et al. (1984), which is proportional to the mass-loss rate of an observed comet. The product of the cometary albedo *A*, dust grain filling factor *f*, and aperture radius ρ, *Af*ρ can be calculated via

$$Af\rho = \frac{4R_H^2 \Delta^2}{\rho} \frac{F_{\text{com}}}{F_{\text{Sun}}}, \qquad (3)$$

where Δ is the geocentric distance of an observed comet (measured in cm), R_H is its heliocentric distance (measured in au), ρ the aperture radius used to measure its brightness (measured in cm), F_{com} is the measured flux of the comet, and F_{Sun} is the solar flux measured at 1 au. This equation can be alternatively expressed in terms of the magnitudes of the comet
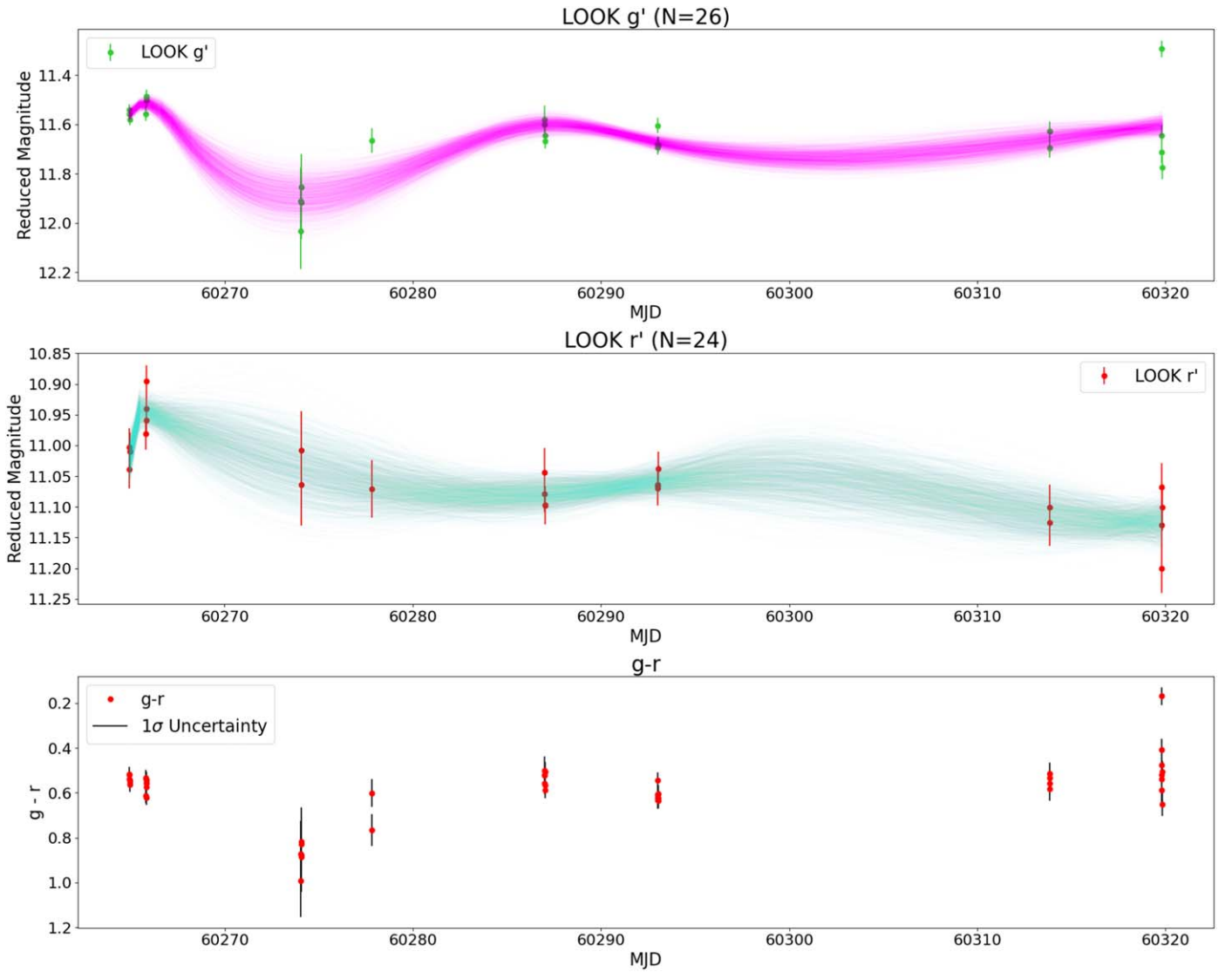
Figure 5. Top: LOOK g-filter reduced magnitudes (green circles) vs. time with third-order interpolated splines fitted to synthetic data overplotted (green). Middle: LOOK r filter reduced magnitudes (red circles) vs. time with third-order interpolated splines fitted to synthetic data overplotted (turquoise). Bottom: $g - r$ color index value calculated from the predicted magnitudes in each filter from the synthetic magnitudes plotted across time. Red circles denote nominal color index values with green lines highlighting the range that includes the central 68.3% of synthetic values.

M_{com} and Sun M_{Sun} as

$$Af\rho = \frac{4R_H^2 \Delta^2}{\rho} 10^{0.4(M_{Sun}-M_{com})}. \quad (4)$$

We use an aperture radius of $\rho = 20,000$ km as per Section 3.1 and the same geocentric and heliocentric distances as used in Section 3.2. The cometary activity levels exhibited by 2023 RN$_3$ are wavelength dependent, as the color of the material emitted by the comet relative to the Sun will have a corresponding effect on the measured $Af\rho$ values. As 2023 RN$_3$ has not undergone any significant color evolution across our data set, we take our lightcurve corrected to the ATLAS o filter from Figure 2 in Section 3.1 to calculate $Af\rho$. For this calculation, we apply the ATLAS o filter solar magnitude measurement of -26.982 (A. F. Gillan et al. 2024). $Af\rho$ is also dependent on the solar phase angle of the comet at the time of measurement due to the light-scattering properties of the coma dust particles. We correct our $Af\rho$ values for effects of phase

angle using the Schleicher–Marcus[14] cometary phase function (D. G. Schleicher et al. 1998; J. N. Marcus 2007; D. Schleicher 2010).

The resulting phase-corrected values, $A(0°)f\rho$, are plotted across time in Figure 8, showing 2023 RN$_3$ to rapidly increase in activity before plateauing around a maximum $A(0°)f\rho$ value of approximately 400 cm for most of our observations. This is consistent with continuous and sustained activity instead of a brief outburst. We consider the continuous nature of 2023 RN$_3$'s cometary activity sufficient to permit comparison of its $Af\rho$ value to other objects. 2023 RN$_3$'s maximum $A(0°)f\rho$ value is greater than that of most JFCs (O. Shubina et al. 2023; A. F. Gillan et al. 2024; T. Kareta et al. 2024) yet is far less than those of outbursts exhibited by the JFC 17P/Holmes (J. M. Trigo-Rodriguez et al. 2008; Z.-Y. Lin et al. 2009; J. M. Trigo-Rodríguez et al. 2010) and the Centaur 29P Schwassman-Wachmann 1 (J. M. Trigo-Rodríguez et al. 2010;

---

[14] https://asteroid.lowell.edu/comet/dustphase/details
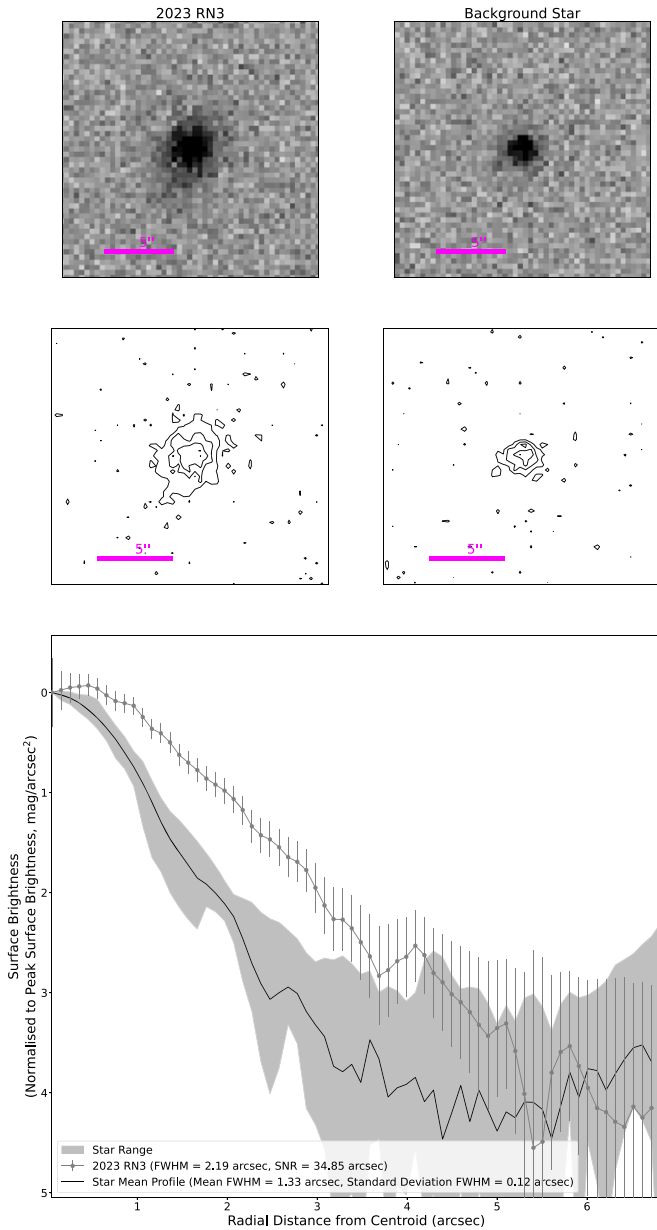
Figure 6. LOOK project contour plots. Top row: 2024 January 4 (MJD 60313.8750614) *i*-filter LOOK observation of 2023 RN$_3$ (left) and a nearby background star (right). Center row: corresponding contour plots of the PSFs of 2023 RN$_3$ (left) and the same background star (right). Bottom: radial profile of 2023 RN$_3$ (gray circles) compared to mean radial profile (black line) and range of profiles (gray shaded) of 10 nearby field stars from 2024 January 4 *i*-filter LOOK observation, plotting instrumental surface brightness (in units of mag arcsec^{-2}) normalized to the peak brightness of 2023 RN$_3$ vs. radial distance from the PSF centroid.

(The complete figure set (41 images) is available in the online article.)

Figure 7. Liverpool Telescope contour plots. Top row: 2023 December 14 (MJD 60292.826273) SDSS-I filter Liverpool Telescope observation of 2023 RN$_3$ (left) and a nearby background star (right). Center row: corresponding contour plots of the PSFs of 2023 RN$_3$ (left) and the same background star (right). Bottom: radial profile of 2023 RN$_3$ (gray circles) compared to mean radial profile (black line) and range of profiles (gray shaded) of 10 nearby field stars from 2023 December 14 SDSS-I filter LOOK observation, plotting instrumental surface brightness (in units of mag arcsec^{-2}) normalized to the peak brightness of 2023 RN$_3$ vs. radial distance from the PSF centroid.

(The complete figure set (12 images) is available in the online article.)

Z.-Y. Lin 2023), which increased the apparent brightness of the respective objects by several magnitudes, and whose maximum $Af\rho$ values were of the order of 10^3–10^5 cm. This difference in $Af\rho$ values may be due to different sizes or numbers of active regions on the objects' surfaces, though a comparison of such active regions is beyond the scope of this paper.

3.5. Orbital Evolution

As mentioned above, E. Lilly et al. (2024) found evidence that cometary activity in Centaurs and high-perihelion JFCs may be triggered by rapid changes in semimajor axis due to planetary perturbations. To investigate this possibility for 2023 RN$_3$, we performed an *N*-body simulation using *REBOUND* (H. Rein & S. F. Liu 2012) and *astropy* (Astropy Collaboration et al. 2013, 2018, 2022). We obtained the most recent orbital elements with epoch JD 2460222.5 $\equiv$ 2023.759 TDB from the JPL solar system Database via the JPL SSDB Application Programming Interface, calculated from observations up to 13 January 2024, and generated an additional 100 clones using the associated covariance matrix. Including the eight major planets, we integrated all bodies for ±500 yr from the orbital epoch
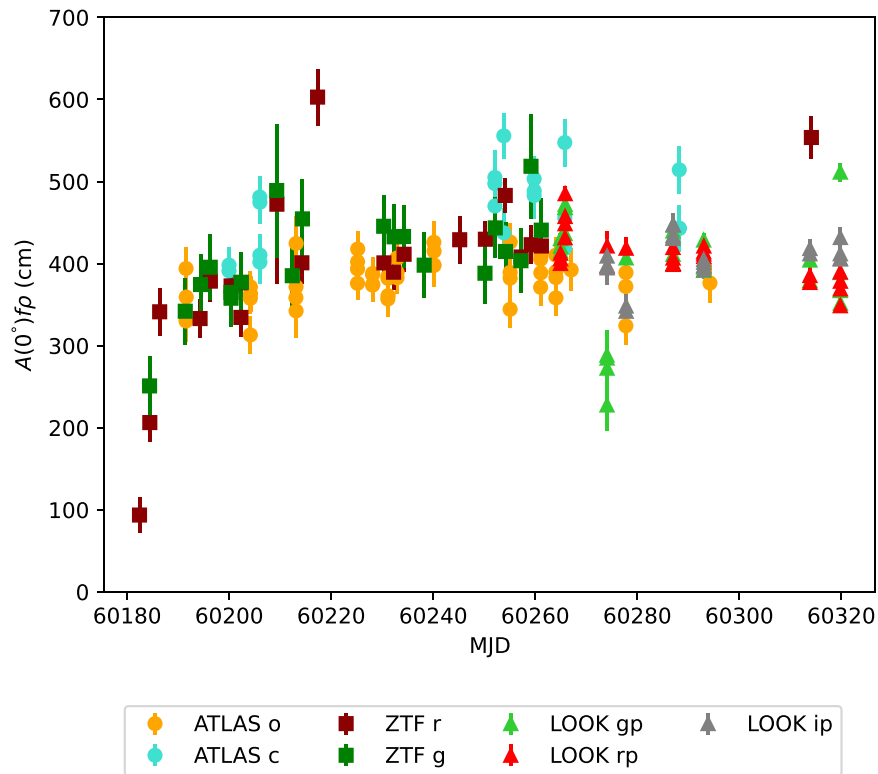
Figure 8. $A(0°)f\rho$ values of 2023 RN$_3$ across time. $A(0°)f\rho$ values have been corrected for color and phase effects.

using the IAS15 integrator (H. Rein & D. S. Spiegel 2015). The resulting orbital evolution of all 101 test objects are shown in Figure 9. We found that the orbit of 2023 RN$_3$ is well constrained between the years 1549 and 2388. Planetary encounters on those dates significantly increase orbital uncertainties outside this date range. At the current epoch, 2023 RN$_3$ has just experienced a rapid increase in semimajor axis of $\Delta a = +0.3$ au due to a distant encounter with Jupiter, with a small simultaneous increase in eccentricity e maintaining the same perihelion distance q. We note that E. Lilly et al. (2024) found almost all activity in Centaurs correlated with rapid *decreases* in a, with only 4 out of 56 objects having undergone increases in a. The most similar object in their study was C/2013 P4 (Pan-STARRS), which also underwent $\Delta a = +0.3$ au 176 yr ago, although of course we have no information on its activity at that time. Hence, it is unclear whether this small 3% increase in a would or could lead to the sudden onset of significant activity observed by us in 2023 RN$_3$.

4. Summary and Conclusions

We analyzed the 2023 cometary activity of the JFC 2023 RN$_3$ using serendipitous observations from the ATLAS and ZTF surveys combined with targeted follow-up observations from LOOK and the Liverpool Telescope. This resulted in a lightcurve spanning 7 months of high-cadence observations. We used this lightcurve of 2023 RN$_3$ to analyze its evolution in brightness, color index, and activity levels. We also utilized our higher-resolution observations from LOOK and the Liverpool Telescope to analyze the radial profile of 2023 RN$_3$. Our key findings are as follows:

1. The lightcurve of 2023 RN$_3$ is indicative of the onset of an epoch of continuous cometary activity, commencing about 10 days before its first detection on 2023 August

26, and reaching a maximum brightness of about 17.5 mag, corresponding to a brightness increase of $\geqslant 5.4$ mag based on upper limits from H. H. Hsieh et al. (2023).

2. We do not observe any significant change in color across our observations.

3. Analysis of 2023 RN$_3$'s surface brightness radial profile shows significant extension compared to background stars, indicating the presence of a spatially extended coma, consistent with H. H. Hsieh et al. (2023).

4. We measure a maximum dust-production rate of $A(0°)f\rho \sim 400$ cm, larger than that of most JFCs, but smaller than that observed for the outbursts of 29P and 17P.

5. We find that 2023 RN$_3$ has experienced an increase in semimajor axis of $a = +0.3$ au due to a planetary encounter with Jupiter, coinciding with its current active epoch.

With a heliocentric distance at the time of its detected onset of cometary activity of 5.301 au, 2023 RN$_3$ resides beyond the so-called "ice line" at $\sim$3 au, interior to which direct sublimation of water ice is the dominant mechanism for observed cometary activity (K. J. Meech & J. Svoren 2004; M. Womack et al. 2017). This rules out direct sublimation of water ice as the mechanism behind 2023 RN$_3$'s 2023 cometary activity. Possible drivers of this cometary activity could be the volatile species of CO or CO_2, which are thought to dominate observed cometary activity beyond the ice line (M. F. A'Hearn et al. 2012; T. Ootsubo et al. 2012; W. T. Reach et al. 2013; J. M. Bauer et al. 2015; A. L. Cochran et al. 2015; M. Womack et al. 2017). While we have shown that 2023 RN$_3$ has recently experienced a slight increase in semimajor axis due to a
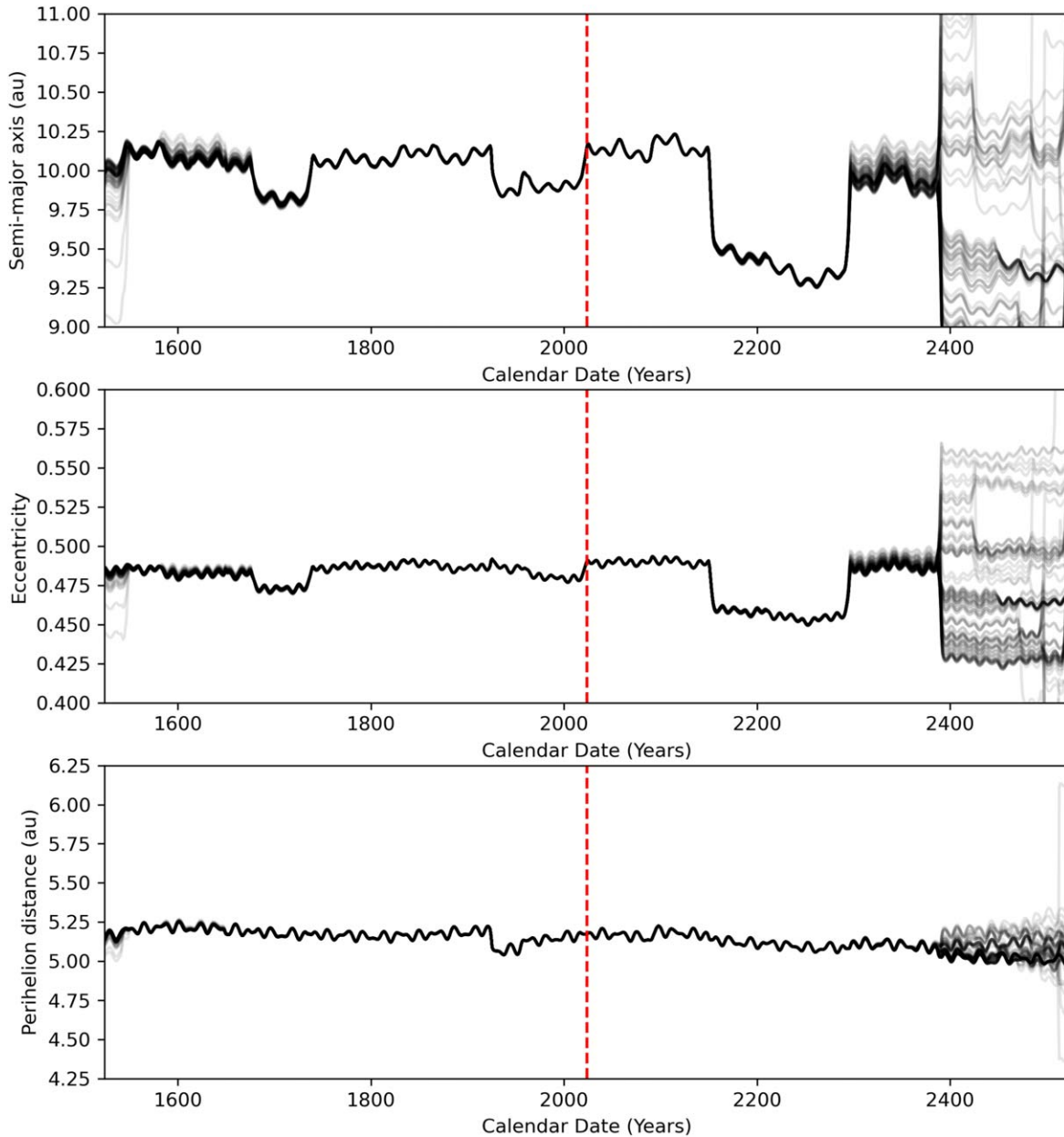
Figure 9. Orbital evolution calculations of the 2023 RN$_3$ nominal orbit and 100 clones. Top panel: semimajor axis a vs. date. The red dashed line indicates the starting epoch of the orbital integrations. The y-axis range of the top panel has been chosen to clearly show the small jumps in a near the current epoch. Middle and bottom panels: as for the top panel, but showing eccentricity e and perihelion distance q.

planetary encounter, whether this has led to the observed onset of cometary activity remains ambiguous as cometary activity in Centaurs and JFCs triggered by planetary encounters is normally associated with rapid decreases in the objects' semimajor axes (E. Lilly et al. 2024). The lack of any detected periodic outbursts by 2023 RN$_3$ may be due to its nucleus having a bilobate structure akin to that of 29P/Schwassman-Wachmann 1 (S. Faggi et al. 2024), shielding a possible patch of volatiles from direct insolation until the onset of its recent active epoch. Confirmation of the nuclear shape of 2023 RN$_3$ via lightcurve analysis or direct imaging could help test this theory.

Estimates of the maximum dust-production levels across 2023 RN$_3$'s 2023 cometary activity are considerably smaller than those of cometary outbursts with similar changes in brightness. 2023 RN$_3$'s $Af\rho$ maximum is consistent with the

JFC population as a whole (O. Shubina et al. 2023; A. F. Gillan et al. 2024; T. Kareta et al. 2024), albeit at the high end of the distribution, and is also consistent with those exhibited by the Centaur population (ranging from $\sim 10^2$–10^5 cm). This further highlights 2023 RN$_3$'s relevance to the study of cometary activity in both these populations.

We highlight that this object, and its corresponding cometary activity, was detected via serendipitous observations from ATLAS. The upcoming Legacy Survey of Space and Time (LSST) by the Vera C. Rubin Observatory (LSST Science Collaboration et al. 2009; Ž. Ivezić et al. 2019; M. Jurić et al. 2019; M. E. Schwamb et al. 2023), with its high observation cadence and faint limiting magnitude, will allow us to track the continued brightness evolution of 2023 RN$_3$ and detect any changes in activity such as future cometary outbursts. LSST's faint limiting magnitude of ~ 24 mag (F. B. Bianco et al. 2022)

will allow us to discover many more such instances of cometary activity across the solar system, helping us to further shed light on the evolution of short period comets.

ORCID iDs

Matthew M. Dobson ⓘ https://orcid.org/0000-0002-1105-7980
Megan E. Schwamb ⓘ https://orcid.org/0000-0003-4365-1455
Alan Fitzsimmons ⓘ https://orcid.org/0000-0003-0250-9911
Michael S. P. Kelley ⓘ https://orcid.org/0000-0002-6702-7676
Carrie E. Holt ⓘ https://orcid.org/0000-0002-4043-6445
Joseph Murtagh ⓘ https://orcid.org/0000-0001-9505-1131
Henry H. Hsieh ⓘ https://orcid.org/0000-0001-7225-9271
Larry Denneau ⓘ https://orcid.org/0000-0002-7034-148X
Nicolas Erasmus ⓘ https://orcid.org/0000-0002-9986-3898
A. N. Heinze ⓘ https://orcid.org/0000-0003-3313-4921
Luke J. Shingles ⓘ https://orcid.org/0000-0002-5738-1612
Robert J. Siverd ⓘ https://orcid.org/0000-0001-5016-3359
Ken W. Smith ⓘ https://orcid.org/0000-0001-9535-3199
John L. Tonry ⓘ https://orcid.org/0000-0003-2858-9657
Henry Weiland ⓘ https://orcid.org/0000-0003-1847-9008
David. R. Young ⓘ https://orcid.org/0000-0002-1229-2499
Tim Lister ⓘ https://orcid.org/0000-0002-3818-7769
Edward Gomez ⓘ https://orcid.org/0000-0001-5749-1507
Joey Chatelain ⓘ https://orcid.org/0000-0002-1278-5998
Sarah Greenstreet ⓘ https://orcid.org/0000-0002-4439-1539

References

A'Hearn, M. F., Feaga, L. M., Keller, H. U., et al. 2012, ApJ, 758, 29
A'Hearn, M. F., Schleicher, D. G., Millis, R. L., Feldman, P. D., & Thompson, D. T. 1984, AJ, 89, 579
Astropy Collaboration, Price-Whelan, A. M., Lim, P. L., et al. 2022, ApJ, 935, 167
Astropy Collaboration, Price-Whelan, A. M., Sipőcz, B. M., et al. 2018, AJ, 156, 123
Astropy Collaboration, Robitaille, T. P., Tollerud, E. J., et al. 2013, A&A, 558, A33
Barbary, K. 2016, JOSS, 1, 58
Barnsley, R. M., Jermak, H. E., Steele, I. A., et al. 2016, JATIS, 2, 015002
Bauer, J. M., Grav, T., Blauvelt, E., et al. 2013, ApJ, 773, 22
Bauer, J. M., Stevenson, R., Kramer, E., et al. 2015, ApJ, 814, 85
Bellm, E. C., Kulkarni, S. R., Graham, M. J., et al. 2019, PASP, 131, 018002
Bertin, E., & Arnouts, S. 1996, A&AS, 117, 393
Bianco, F. B., Ivezić, Ž., Jones, R. L., et al. 2022, ApJS, 258, 1
Bradley, L. 2023, astropy/photutils: v1.8.0, Zenodo, doi:10.5281/zenodo.7946442
Brown, T. M., Baliber, N., Bianco, F. B., et al. 2013, PASP, 125, 1031
Chambers, K. C., Magnier, E. A., Metcalfe, N., et al. 2016, arXiv:1612.05560

Cochran, A. L., Levasseur-Regourd, A.-C., Cordiner, M., et al. 2015, SSRv, 197, 9

Dobson, M. M., Schwamb, M. E., Fitzsimmons, A., et al. 2024, PSJ, 5, 165

Faggi, S., Villanueva, G. L., McKay, A., et al. 2024, NatAs, 8, 1237

Fernández, J. A., Helal, M., & Gallardo, T. 2018, P&SS, 158, 6

Flewelling, H. A., Magnier, E. A., Chambers, K. C., et al. 2020, ApJS, 251, 7

Gillan, A. F., Fitzsimmons, A., Denneau, L., et al. 2024, PSJ, 5, 25

Gladman, B., Marsden, B. G., & Vanlaerhoven, C. 2008, in Nomenclature in the Outer Solar System, ed. M. A. Barucci et al. (Tucson, AZ: Univ. Arizona Press), 43

Graham, M. J., Kulkarni, S. R., Bellm, E. C., et al. 2019, PASP, 131, 078001

Green, D. W. E. 2023, COMET C/2023 RN3 (ATLAS)

Harris, C. R., Millman, K. J., van der Walt, S. J., et al. 2020, Natur, 585, 357

Hsieh, H. H., Kelley, M. S. P., Lister, T. A., et al. 2023, RNAAS, 7, 263

Hughes, D. W. 1990, QJRAS, 31, 69

Hunter, J. D. 2007, CSE, 9, 90

Ivezić, Ž, Kahn, S. M., Tyson, J. A., et al. 2019, ApJ, 873, 111

Jewitt, D. 2009, AJ, 137, 4296

Jewitt, D., & Hsieh, H. H. 2022, arXiv:2203.01397

Joye, W. 2019, SAOImageDS9/SAOImageDS9 v8.0.1, Zenodo, doi:10.5281/zenodo.2530958

Jurić, M., Jones, R. L., Bryce Kalmbach, J., et al. 2019, arXiv:1901.08549

Kareta, T., Noonan, J. W., Volk, K., Strauss, R. H., & Trilling, D. 2024, ApJL, 967, 11

Kelley, M., & Lister, T. 2021, mkelley/calviacat: v1.2.0, Zenodo, doi:10.5281/zenodo.5061298

Kelley, M. S., & Wooden, D. H. 2009, P&SS, 57, 1133

Kluyver, T., Ragan-Kelley, B., Pérez, F., et al. 2016, in Positioning and Power in Academic Publishing: Players, Agents and Agendas, ed. F. Loizides & B. Scmidt (Amsterdam: IOS Press), 87

Lilly, E., Hsieh, H., Bauer, J., et al. 2021, PSJ, 2, 155

Lilly, E., Jevčák, P., Schambeau, C., et al. 2024, ApJL, 960, L8

Lin, Z.-Y. 2023, PASJ, 75, 462

Lin, Z.-Y., Lin, C.-S., Ip, W.-H., & Lara, L. M. 2009, AJ, 138, 625

Lister, T., Kelley, M. S. P., Holt, C. E., et al. 2022, PSJ, 3, 173

Lister, T. A., Gomez, E., Chatelain, J., et al. 2021, Icar, 364, 114387

LSST Science Collaboration, Abell, P. A., Allison, J., et al. 2009, arXiv:0912.0201

Magnier, E. A., Chambers, K. C., Flewelling, H. A., et al. 2020, ApJS, 251, 3

Manzini, F., Oldani, V., Ochner, P., Bedin, L. R., & Reguitti, A. 2023, ATel, 16194, 1

Marcus, J. N. 2007, ICQ, 29, 39

Masci, F. J., Laher, R. R., Rusholme, B., et al. 2019, PASP, 131, 018003

McCully, C., Volgenau, N. H., Harbeck, D.-R., et al. 2018, Proc. SPIE, 10707, 107070K

Meech, K. J., & Svoren, J. 2004, in Comets II, ed. M. C. Festou, H. U. Keller, & H. A. Weaver (Tucson, AZ: Univ. Arizona Press), 317

Miles, R. 2016, Icar, 272, 387

Ootsubo, T., Kawakita, H., Hamada, S., et al. 2012, ApJ, 752, 15

pandas development team, T 2020, pandas-dev/pandas: Pandas, v2.2.3, Zenodo, doi:10.5281/zenodo.3509134

Peixinho, N., Thirouin, A., Tegler, S. C., et al. 2020, in The Trans-Neptunian Solar System, ed. D. Prialnik, M. A. Barucci, & L. Young (Amsterdam: Elsevier), 307

Prialnik, D. 1992, ApJ, 388, 196

Reach, W. T., Kelley, M. S., & Vaubaillon, J. 2013, Icar, 226, 777

Rein, H., & Liu, S. F. 2012, A&A, 537, A128

Rein, H., & Spiegel, D. S. 2015, MNRAS, 446, 1424

Schleicher, D. 2010, Composite Dust Phase Function for Comets—Lowell Minor Planet Services

Schleicher, D. G., Millis, R. L., & Birch, P. V. 1998, Icar, 132, 397

Schwamb, M. E., Jones, R. L., Yoachim, P., et al. 2023, ApJS, 266, 22

Shubina, O., Kleshchonok, V., Ivanova, O., Luk'yanyk, I., & Baransky, A. 2023, Icar, 391, 115340

Smith, K. W., Smartt, S. J., Young, D. R., et al. 2020, PASP, 132, 085002

Solontoi, M., Ivezić, Ž., Jurić, M., et al. 2012, Icar, 218, 571

Steele, I. A., Smith, R. J., Rees, P. C., et al. 2004, Proc. SPIE, 5489, 679

Tonry, J. L., Denneau, L., Flewelling, H., et al. 2018b, ApJ, 867, 105

Tonry, J. L., Denneau, L., Heinze, A. N., et al. 2018a, PASP, 130, 064505

Tonry, J. L., Stubbs, C. W., Lykke, K. R., et al. 2012, ApJ, 750, 99

Trigo-Rodriguez, J. M., Davidsson, B., Montanes-Rodriguez, P., Sanchez, A., & Troughton, B. 2008, LPSC, 39, 1627

Trigo-Rodríguez, J. M., García-Hernández, D. A., Sánchez, A., et al. 2010, MNRAS, 409, 1682

Trigo-Rodriguez, J. M., García-Melendo, E., Davidsson, B. J. R., et al. 2008, A&A, 485, 599

Trigo-Rodríguez, J. M., Sánchez, A., Llenas, J. M., & Gritsevich, M. 2024, LPSC, 55, 1363

van der Walt, S., Colbert, S. C., & Varoquaux, G. 2011, CSE, 13, 22

Van Rossum, G. 2020, The Python Library Reference, Release 3.8.2 (Python Software Foundation)

Virtanen, P., Gommers, R., Oliphant, T. E., et al. 2020, NatMe, 17, 261

Willmer, C. N. A. 2018, ApJS, 236, 47

Womack, M., Sarid, G., & Wierzchos, K. 2017, PASP, 129, 031001